Journal of Catalysis **209,** 306–317 (2002)
doi:10.1006/jcat.2002.3643

Efficient Production of Hydrogen over Supported Cobalt Catalysts from Ethanol Steam Reforming

Jordi Llorca, Narcís Homs, Joaquim Sales, and Pilar Ramírez de la Piscina[1]

Departament de Química Inorgànica, Facultat de Química, Universitat de Barcelona, C/Martí i Franquès 1-11, 08028 Barcelona, Spain

Received July 25, 2001; revised April 17, 2002; accepted April 23, 2002

The reaction between ethanol and water was studied in the temperature range 573–723 K at atmospheric pressure over supported cobalt catalysts. Cobalt-loaded catalysts (1%) were prepared by impregnation of $Co_2(CO)_8$ on MgO, γ-Al_2O_3, SiO_2, TiO_2, V_2O_5, ZnO, La_2O_3, CeO_2, and Sm_2O_3. Ethanol steam reforming occurred to a large degree over ZnO-, La_2O_3-, Sm_2O_3-, and CeO_2-supported catalysts; CO-free hydrogen was produced. Samples were characterized after catalytic tests by high-resolution transmission electron microscopy, electron diffraction, X-ray diffraction, Raman spectroscopy, X-ray photoelectron spectroscopy, and temperature-programmed hydrogen reaction. Depending on the support, different cobalt-based phases were identified: metallic cobalt particles, Co_2C, CoO, and La_2CoO_4. The extent and nature of carbon deposition depended on the sample and on the reaction temperature. ZnO-supported samples showed the best catalytic performances. Under 100% ethanol conversion, selectivity up to 73.8% to H_2 and 24.2% to CO_2 was obtained. © 2002 Elsevier Science (USA)

Key Words: **hydrogen; ethanol; steam reforming; supported cobalt; fuel cells; oxide supports.**

INTRODUCTION

The production of H_2 from the steam reforming of alcohols could favor the use of H_2 as an alternative fuel, removing the difficulty of storage and distribution. Although the steam reforming of methanol has been widely described (1–4), fewer studies have dealed with ethanol steam reforming (5, 6). However, from an environmental point of view the use of ethanol is preferred, because ethanol could be considered a renewable raw material which can be easily obtained from biomass. Moreover, a high yield of hydrogen can be obtained from the above mentioned reaction:

$$CH_3CH_2OH + 3H_2O \rightarrow 6H_2 + 2CO_2.$$

Recently, we studied the behavior of several oxides in the steam reforming of ethanol. Some of them have shown good performances for the production of CO-free hydrogen, and their catalytic behavior has been related to their redox and acid–base properties (7). On the other hand, cobalt-based catalysts had been proposed as appropriate catalysts for this process (5). As a background in the preparation and behavior of supported cobalt catalysts, we had reported highly selective synthesis of ethanol from the CO hydrogenation over Co/ZnO catalyst prepared by impregnation of $Co_2(CO)_8$ (8). In this work, and on the basis of these results, we extended the preparation method to several oxide supports, with a wide range of redox and acid–base properties, which in turn had previously been studied in the steam reforming of ethanol. The behavior of catalysts on the title reaction was studied and catalysts were characterized by transmission electron microscopy (TEM), electron diffraction (ED), Raman spectroscopy, X-ray photoelectron spectroscopy (XPS), X-ray diffraction (XRD), and temperature-programmed hydrogen reaction (TPHR).

EXPERIMENTAL

Preparation of Catalysts

Supported cobalt catalysts with a ca. 1% metal loading were prepared in a vacuum gas line by impregnation from *n*-hexane $Co_2(CO)_8$ solutions. The supports used were MgO (prepared by adding ammonia to a $MgCl_2$ solution, 110 m^2 g^{-1}), γ-Al_2O_3 (Girdler, 188 m^2 g^{-1}), SiO_2 (Degussa-Hüls, 200 m^2 g^{-1}), TiO_2 (>80% anatase, Degussa–Hüls, 45 m^2 g^{-1}), V_2O_5 (Merck, 22 m^2 g^{-1}), ZnO(1) (Asturienne, New Jersey, 11 m^2 g^{-1}), ZnO(2) (prepared by decomposition of $3ZnO \cdot 2ZnCO_3 \cdot 3H_2O$, 100 m^2 g^{-1}), La_2O_3 (Merck, 11 m^2 g^{-1}), CeO_2 (Aldrich, 17 m^2 g^{-1}), and Sm_2O_3 (Merck, 9 m^2 g^{-1}). Prior to impregnation, supports were partially dehydrated by treatment under high vacuum at 473 K for 16 h. After impregnation and solvent evaporation, the resulting samples were dried at room temperature until a total pressure of ca. 10^{-5} mbar was reached. Chemical analyses performed by inductively coupled plasma atomic absorption revealed that the cobalt contents for all samples were in the range 1.1–1.2 wt%. A sample containing the La_2CoO_4 phase was prepared by the citrate method (9).

[1] To whom correspondence should be addressed. Fax: 34-93-4907725. E-mail: pilar.piscina@qi.ub.es.

0021-9517/02 $35.00

Catalytic Tests

Catalytic studies of ethanol steam reforming were performed at atmospheric pressure in a U-shaped quartz reactor (5-mm internal diameter). The catalyst (100 mg) was charged for each of the reaction tests and diluted with inactive SiC, giving a catalyst bed volume of 0.6 ml. The feed of the reactants comprised a gaseous mixture of ethanol, water, and argon. Ar (purity 99.9995%) was supplied by a mass flow controller. A constant mixture of $EtOH : H_2O = 20 : 80$ by volume ($EtOH : H_2O \sim 1 : 13$ molar basis, HPLC purity grade) was supplied by a Gilson 307 Piston Pump, and the mixture was vaporized at 453 K and mixed with the Ar flow before entering the reaction chamber.

The temperature of the catalyst was raised to 573 K under Ar. Then the $EtOH + H_2O$ mixture was introduced and the temperature increased to that of the catalytic test. All catalysts were tested from 573 to 723 K, with the temperature increased stepwise from 573 to 623, 673, and 723 K. The catalyst was held at each temperature for 2 h (573 and 623 K) and 20 h (673 and 723 K). At the end of the catalytic test the flow of $EtOH + H_2O$ was stopped and the catalyst was cooled under Ar stream and stored for characterization.

Over ZnO-supported catalysts, additional catalytic tests were carried out at 723 K, with variation in the contact time and/or the $Ar/(EtOH + H_2O)$ ratio. In this case, products were analyzed 1 h after each change in the reaction conditions.

The analysis of the reactants and all the reaction products was carried out online by gas chromatography (Varian apparatus). Inside an automated injection valve, the sample was divided into two aliquots which were then analyzed in a different way in order to obtain accurate, complete quantification of the reaction products. One of the aliquots was used to analyze hydrogen, carbon monoxide, carbon dioxide, methane, and water. Argon was used as a carrier gas and separation was accomplished by using a 5-Å molecular sieve and a 6-m-long Hayesep packed column. Hydrogen was quantified with a thermal conductivity detector whereas carbon monoxide, carbon dioxide, and methane were analyzed by a flame ionization detector after being passed through a methanizer device, which contained a nickel catalyst. The detection limit of carbon monoxide was 17 ppm. The other aliquot was used to analyze hydrocarbons and oxygenated products. Helium was used as a carrier gas and separation and quantification were attained by a 100-m-long DB-5 capillary column and a flame ionization detector. Response factors for all products were obtained and the system was calibrated with appropriate standards before each catalytic test.

Catalysts Characterization

Catalysts were studied by TEM techniques, basically in bright field and high resolution, as well as by electron diffraction in convergent-beam (CBED) and selected-area modes (SAED). Samples were deposited on copper grids with a holey carbon-film support. The instrument used was a Philips CM-30 electron microscope equipped with a LaB_6 source and working at 300 kV, with a point-to-point resolution of 0.19 nm. Magnification and camera constants were calibrated using appropriate standards under the same electron-optical conditions. In some cases, Fourier transformed images were obtained by using local software on digitalized parts of the negatives.

XRD profiles were collected at a step width of 0.02 degrees and by counting 10 s at each step using a Siemens D-500 X-ray diffractometer equipped with a Cu target and a graphite monochromator.

TPHR was followed using a Balzers QMS 200 quadrupole mass spectrometer. The experiments were performed over postreaction samples pretreated in He at 873 K by using a constant flow of H_2 diluted in He (20 ml min^{-1}) at a heating rate of 2 K min^{-1}up to 873 K.

XP spectra were recorded with a Perkin–Elmer PHI-5500 spectrometer equipped with an Al X-ray source and a hemispherical electron analyzer. The X-ray source was operated at 12.4 kV. The binding energy (BE) reference was taken at the Zn 2p peak from ZnO at 1022.0 eV. The accuracy of the binding energy was within 0.1 eV.

Raman spectroscopy was performed with a Jobin Yvon T64000 instrument using an Ar ion laser as an illumination source (514.5 nm) and a CCD detector cooled at 140 K. The Raman instrument was coupled to a standard Olympus microscope ($\times 50$ magnification) and the collection optics system was used in the backscattering configuration. The laser power at the sample was limited to 3 mW in order to avoid laser heating effects.

RESULTS AND DISCUSSION

Ethanol Steam-Reforming Reaction

The ethanol steam-reforming reaction was studied under a mixture $1 : 13 : 70$ $EtOH : H_2O : Ar$ (molar ratio), between 573 and 723 K, at atmospheric pressure. Figure 1 shows for each sample values of ethanol conversion and H_2 and CO_2 production as a function of reaction temperature and time. Ethanol conversion and CO_2 and H_2 production increased with temperature for all catalysts. The values obtained at 723 K along time show a severe decrease in ethanol conversion for Co/TiO_2 and a slight deactivation for Co/MgO, Co/SiO_2, Co/CeO_2, and Co/Sm_2O_3 samples.

Table 1 shows conversion and selectivity values obtained after 20 h at 723 K (total reaction time, 50 h). These data allow evaluation of the extent of the ethanol steam-reforming reaction, $CH_3CH_2OH + 3H_2O \rightarrow 6H_2 + 2CO_2$, and that of the other ethanol reactions which took place over the catalysts: mainly, ethanol decomposition to CH_4,$CH_3CH_2OH \rightarrow CO + CH_4 + H_2$; ethanol dehydration to ethylene; ethanol dehydrogenation to acetaldehyde;

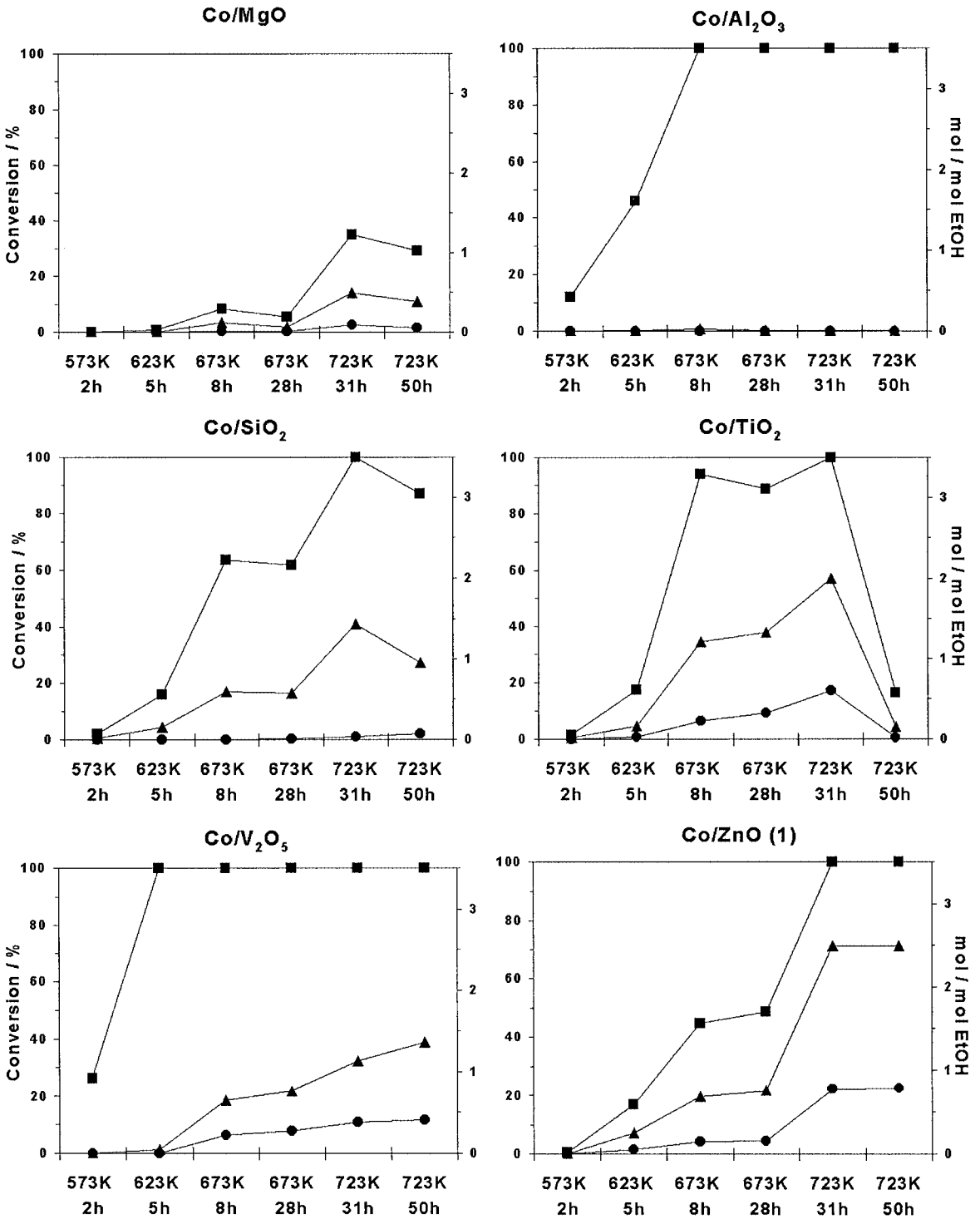

FIG. 1. Ethanol conversion and H_2 and CO_2 production over supported cobalt catalysts as a function of temperature and reaction time. Reaction conditions: total pressure, 1 atm; $EtOH:H_2O:Ar = 1:13:70$ (molar ratio), $GHSV = 5000\ h^{-1}$. (■) Ethanol conversion; (▲) mol H_2/mol EtOH; (●) mol CO_2/mol EtOH.

ethanol decomposition to acetone, $2CH_3CH_2OH \rightarrow CH_3COCH_3 + CO + 3H_2$; and water–gas shift reaction, $CO + H_2O \rightarrow CO_2 + H_2$. Table 1 also lists mean cobalt particle size as determined by TEM after reaction at 723 K.

Negligible steam reforming of ethanol was observed over Co/Al_2O_3. The dehydration of ethanol to ethylene took place to a large extent according to the behavior of Al_2O_3 under similar conditions and with its acidic characteristics (7, 10).

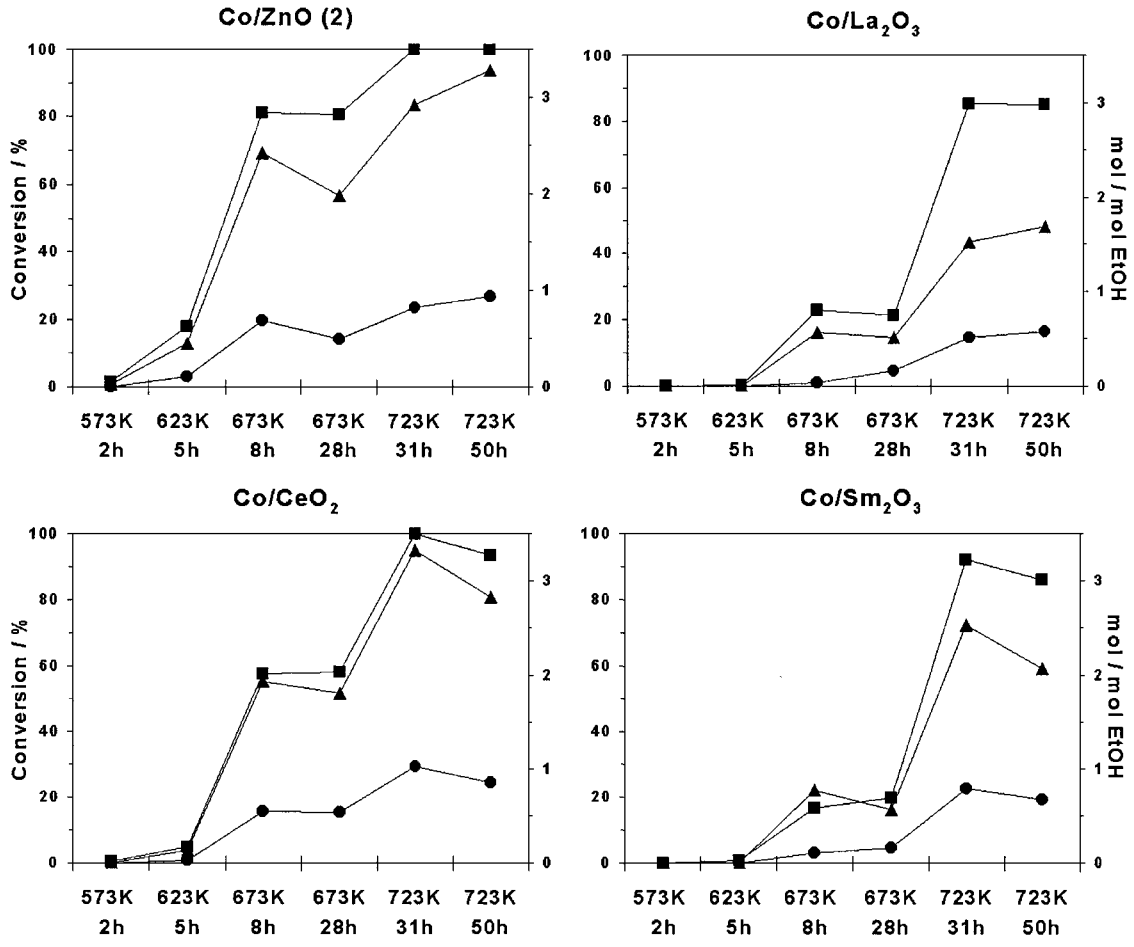

FIG. 1—*Continued*

Co/MgO catalyst showed the smallest initial conversion at each temperature (see Fig. 1); this catalyst only gave around 30% conversion of ethanol at the highest temperature (723 K) studied. The selectivity values indicated that the main reaction that took place over Co/MgO was the dehydrogenation of ethanol to acetaldehyde. However, over this catalyst the ethanol steam-reforming reaction, the ethanol decomposition to methane, and the ethanol

TABLE 1

Catalytic Performance of Supported Cobalt Catalysts and Mean Particle Size of Cobalt Particles Determined by TEM after 20 h at 723 K on a EtOH + H_2O + Ar Stream (EtOH : H_2O : Ar = 1 : 13 : 70 molar ratio) at Atmospheric Pressure and GHSV = 5000 h^{-1}

Catalyst	Conv. (%)	Selectivity[a] (%)								d_{Co} (nm)
		H_2	CO	CO_2	CH_4	C_2H_4	C_3H_6	CH_3CHO	Me_2CO	
Co/MgO	29.3	55.0	0.4	8.2	2.1	2.5	4.2	27.6	—	—
Co/Al_2O_3	100	0.8	—	0.3	0.1	98.8	—	—	—	—
Co/SiO_2	87.0	49.8	2.9	3.9	2.1	3.4	0.2	37.7	—	—
Co/TiO_2	16.4	47.4	—	4.4	0.3	13.5	—	34.4	—	—
Co/V_2O_5	100	53.5	—	16.1	1.2	19.9	0.3	6.4	2.6	3.4
Co/ZnO(1)	100	66.0	—	20.8	0.7	1.1	0.5	4.8	6.1	3.6
Co/ZnO(2)	100	71.3	—	20.2	0.8	0.6	0.1	0.2	6.8	3.5
Co/La_2O_3	85.0	63.1	—	21.5	1.3	1.1	0.1	0.5	12.4	6.1
Co/CeO_2	93.7	69.6	—	21.1	0.1	1.9	0.1	0.8	6.4	7.5
Co/Sm_2O_3	85.9	64.7	—	21.0	1.6	7.3	0.1	—	5.3	3.9

[a] Water not included.

TABLE 2

Catalytic Performance of Co/ZnO(2) at 723 K and Atmospheric Pressure under a Constant EtOH + H_2O Feed (EtOH : H_2O = 1 : 13 Molar Ratio)

GHSV (h^{-1})	Ar/EtOH + H_2O	Conv. (%)	Selectivity[a] (%)								Mol H_2/ mol EtOH	Mol CO_2/ mol EtOH
			H_2	CO	CO_2	CH_4	C_2H_4	C_3H_6	CH_3CHO	Me_2CO		
2,300	2	100	65.7	—	21.6	0.8	1.3	0.2	1.6	8.8	2.4	0.8
3,800	4	100	68.7	—	21.4	0.7	1.1	0.1	0.6	7.4	2.9	0.9
6,800	8	100	69.5	—	22.6	0.6	0.9	0.1	0.7	5.6	3.2	1.0
9,900	12	100	69.9	—	22.7	0.5	1.2	0.2	0.6	4.9	3.3	1.1
12,900	16	100	71.6	—	22.8	0.4	1.2	0.1	0.5	3.4	3.9	1.2
16,000	20	100	72.0	—	23.2	0.4	1.2	—	0.8	2.4	4.1	1.3
19,000	24	100	73.4	—	23.7	0.3	0.9	—	0.5	1.2	4.9	1.6
22,000	28	100	73.8	—	24.2	0.3	0.8	—	—	0.9	5.1	1.7

[a] Water not included.

dehydration were also produced. The dehydrogenation of ethanol to acetaldehyde was also the main reaction observed over MgO, but a maximum conversion value of 6.7% was attained at 723 K and no steam reforming of ethanol took place (7).

Dehydrogenation of ethanol to acetaldehyde was also the main reaction for Co/SiO_2, which showed a selectivity pattern similar to Co/MgO; the conversion values were much higher than over SiO_2 (7).

Co/V_2O_5 required the lowest temperature (623 K) to attain 100% ethanol conversion (Fig. 1). Although the dehydration of ethanol to ethylene was the reaction which took place to the highest extent, 15.7% of the ethanol reacted over Co/V_2O_5 was through the steam-reforming reaction.

Co/ZnO(1), Co/ZnO(2), Co/La_2O_3, Co/CeO_2, and Co/Sm_2O_3 showed selectivity to H_2 higher than 60% and to CO_2 higher than 20%. Over these catalysts the main reactions were the steam reforming of ethanol and the ethanol decomposition to acetone. Co/La_2O_3, Co/CeO_2, and Co/Sm_2O_3 catalysts showed higher conversion values than La_2O_3, CeO_2, and Sm_2O_3, respectively. The selectivity patterns of these catalysts were also different from those of the oxide supports (7); supported cobalt catalysts showed higher selectivity to H_2 and CO_2 and lower selectivity to ethylene.

Co/ZnO(2) exhibited the highest catalytic performance of all catalysts studied (see Fig. 1 and Table 1). In the experimental conditions used, total conversion of ethanol and the highest values of H_2 and CO_2 per mole of reacted EtOH were obtained and no deactivation was observed. When a similar test was carried out over the ZnO(2) support at 723 K, 100% ethanol conversion was also reached but a lower yield on H_2 and CO_2 was obtained (7).

On the other hand, over the Co/ZnO(2) catalyst the decomposition of ethanol to acetone was high. Taking into account the fact that this reaction results from several successive reactions, such as dehydrogenation and aldol condensation (7, 11, 12), several catalytic tests were carried out with variations in the contact time and/or the Ar/(EtOH + H_2O) ratio. Table 2 reports the catalytic performance at 723 K of Co/ZnO(2) under a mixture of Ar : EtOH : H_2O obtained by dilution with Ar of a constant feed of EtOH : H_2O = 1 : 13 (molar ratio). Total conversion was attained in all cases and no carbon monoxide was detected (detection limit, 17 ppm). Short contact times and high Ar/(EtOH + H_2O) ratios favored the reforming reaction over the decomposition to acetone, and in the best case only 2% of the total products were other than H_2 and CO_2.

In order to gain further insight, two different catalytic tests were carried out with the same catalyst at 723 K, where either the contact time or the Ar/(EtOH + H_2O) ratio was kept constant; in both cases a molar ratio EtOH : H_2O = 1 : 13 was used (Fig. 2). Figure 2A corresponds to the experiment carried out at a fixed Ar/(EtOH + H_2O) molar ratio of 5 and with variations in the gas hourly space velocity (GHSV) from 30,000 to 1,250 h^{-1}. Up to 15,000 h^{-1} the extent of the decomposition of ethanol to acetone decreases gradually while the extent of the reforming reaction increases. At higher GHSV values conversion of ethanol is not complete and acetaldehyde is produced, in accordance with a reaction scheme in which ethanol is first dehydrogenated to acetaldehyde. On the other hand, the effect of the Ar/(EtOH + H_2O) ratio is shown in Fig. 2B, where a series of experiments were performed at a fixed GHSV value of 5000 h^{-1}. As the EtOH + H_2O mixture is more diluted in the carrier, the reforming reaction takes place preferentially, and the ethanol decomposition to acetone via aldol condensation of acetaldehyde is depressed. Again, when total conversion of ethanol is not attained, acetaldehyde is observed.

Characterization of Catalysts

TEM studies were carried out on the catalysts after being tested for 50 h in a EtOH + H_2O + Ar stream with

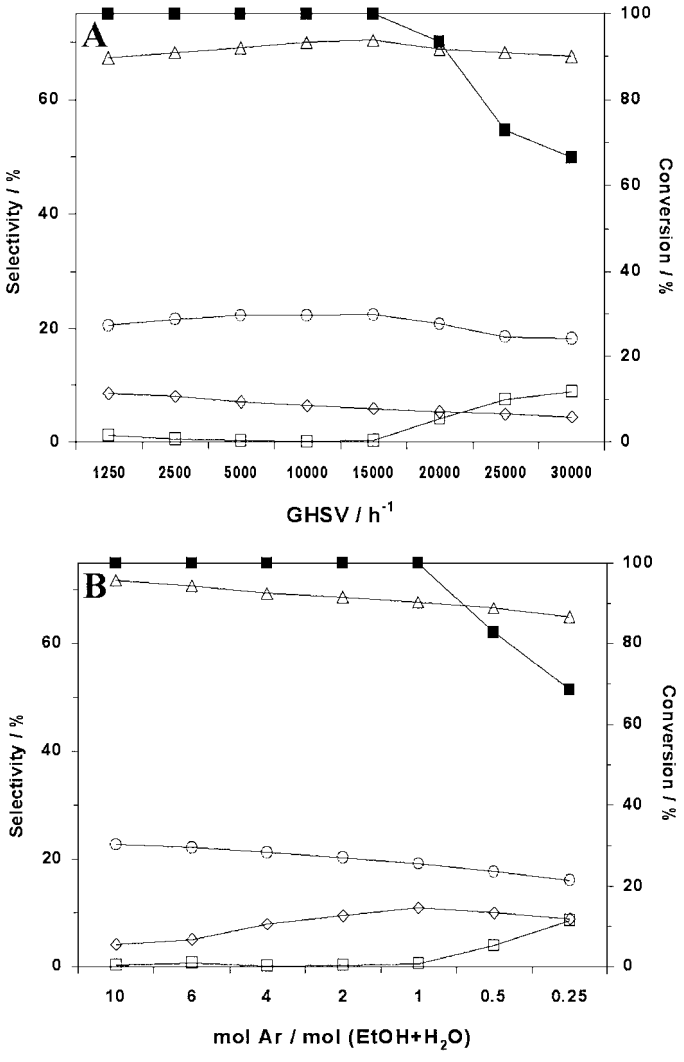

FIG. 2. Catalytic performance of Co/ZnO(2) at 723 K and atmospheric pressure. (A) As a function of GHSV, $EtOH:H_2O:Ar = 1:13:70$ molar ratio. (B) As a function of $Ar/EtOH + H_2O$ ratio, GHSV = 5000 h^{-1}, $EtOH:H_2O = 1:13$ molar ratio. (■) Ethanol conversion. Selectivities: (△) H_2; (○) CO_2; (□) CH_3CHO; (◇) Me_2CO.

$Ar/(EtOH + H_2O) = 5$ molar ratio and 5000 h^{-1} GHSV at increasing temperatures from 573 to 723 K, as detailed under Experimental. Several phases were systematically checked for their presence, including carbon (graphite as well as poorly ordered carbon), metallic cobalt (both cubic and hexagonal phases), cobalt oxides, cobalt carbides, and mixed alloys and oxides which could be obtained from cobalt and the oxide supports.

We could not identify any cobalt-based phase or carbon deposition on Co/MgO and Co/Al_2O_3 catalysts. Taking into account the low metal loading used in our study, the entry of cobalt into the lattice of Al_2O_3 and the formation of nonreducible aluminate may be favored on Co/Al_2O_3 (13); this phase could be not active in the ethanol steam-reforming reaction according to the catalytic results. Over Co/MgO, the formation of MgO–CoO solid solution is likely to occur (14).

The characterization of Co/SiO_2 allowed us to identify CoO particles and abundant carbon deposition on the silica. Figure 3 shows a bright-field image of this sample along with selected-area electron diffraction (SAED) patterns recorded on the silica support and on the metal particles, which are visible in the bright-field image. Diffuse rings corresponding to poorly graphitized carbon are visible in the SAED pattern recorded on silica, whereas defined rings corresponding to multiple particles of the cobalt oxide CoO are identified sitting on the silica support.

High carbon deposition was observed on Co/TiO_2; a 10-nm-thick amorphous layer was clearly visible covering both TiO_2 and cobalt-based particles (see inset in Fig. 4). A lattice-fringe image of this catalyst is shown in the same figure, where a 3.6-Å spacing for C(002), characteristic of poorly graphitized carbon, is visible. At the same time, cobalt-containing particles of about 20 nm appeared, like the one showed in the figure. Convergent-beam electron diffraction of this individual particle (inset) showed that it was Co_2C carbide. These characterization data are consistent with the severe decrease observed on ethanol conversion after 20 h under reaction at 723 K.

TEM analysis of Co/La_2O_3 catalyst showed the presence of aggregates on the La_2O_3 support. Figure 5A corresponds to a high-resolution image of one of these aggregates, where cobalt and the support originated a mixed oxide phase with a spinel structure, La_2CoO_4. This new phase consisted of individual crystals of about 4–6 nm and was located on top

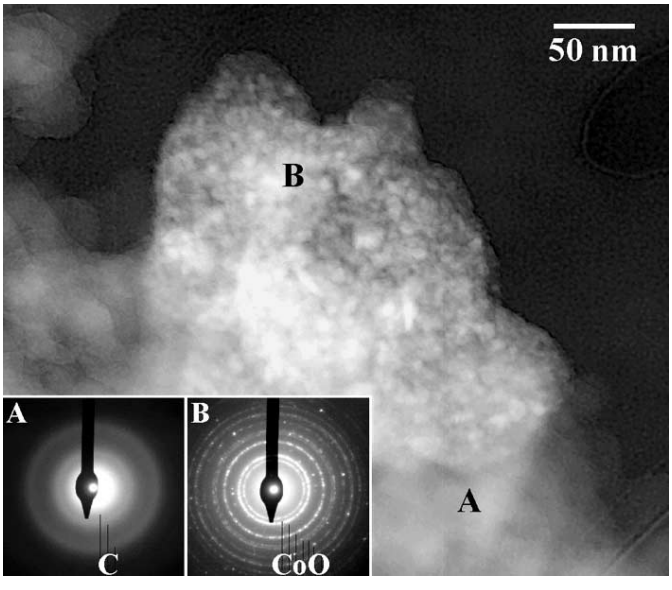

FIG. 3. Bright-field transmission electron microscopy image corresponding to the Co/SiO_2 catalyst. The two insets correspond to selected-area electron diffraction patterns recorded on the silica support alone (A) and on silica-supported cobalt-containing particles (B).

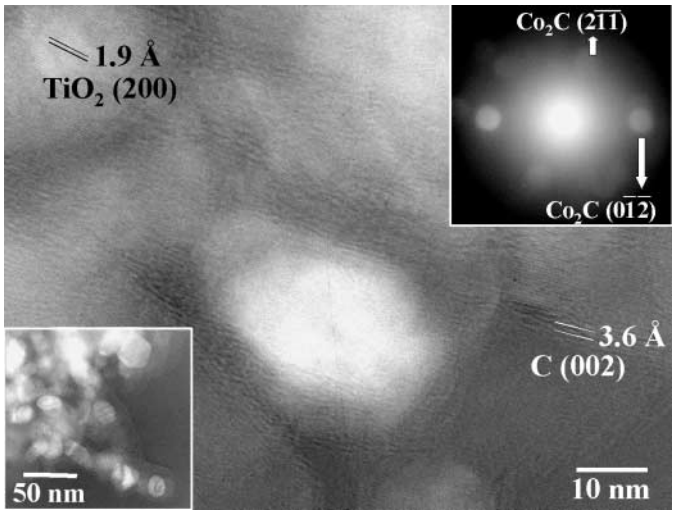

FIG. 4. Images corresponding to the Co/TiO_2 catalyst. A Co_2C carbide phase is identified by means of convergent-beam electron diffraction. The lattice-fringe image shows the presence of TiO_2 support particles and cobalt-based particles covered by a poorly graphitic carbon.

of the support. Two insets in Fig. 5A show La_2CoO_4 particles with distinctive spacing and reciprocal space patterns as obtained by Fourier transformed processing. On the other hand, discrete amorphous carbon deposition was observed on the La_2O_3 support, which is visible directly in the high-resolution image as well as in the Fourier transformed image in another inset of Fig. 5A. In contrast, the La_2CoO_4 crystals appeared free from any carbonaceous layer. In addition to La_2CoO_4, the Co/La_2O_3 catalyst also contained metallic cobalt. Figure 5B corresponds to another aggregate of this catalyst, where different nanometer-size cobalt crystallites are located on top of the aggregate, as evidenced by Fourier transform image.

In order to study the role of the La_2CoO_4 phase identified in the Co/La_2O_3 catalyst in the ethanol steam-reforming reaction, we synthesized a new mixed oxide catalyst which contained the phase La_2CoO_4. The catalytic performance of this sample toward ethanol steam reforming was poorer than that of Co/La_2O_3, where cobalt particles were identified after reaction.

On Co/V_2O_5 vesicular, amorphous carbon covered all the V_2O_5 support, as illustrated in Fig. 6, which corresponds to a bright-field image. In some areas the vesicular carbon contained cobalt particles of about 2–3 nm with a cubic structure, as shown in the inset of Fig. 6, and the empty vesicles marked by white arrows may have been once occupied by such cobalt particles.

TEM analysis of Co/CeO_2 catalyst revealed the presence of aggregates on the surface of CeO_2 with a layered structure, with a more electron-dense core covered by a shell. Lattice-fringe imaging of the aggregates showed that a metallic cobalt core with cubic structure was covered by amorphous carbon. Figure 7 shows a high-resolution image of an aggregate under two different focus conditions. In Fig. 7A, planes corresponding to the spacing of cubic Co(111) are seen along with CeO_2 (111) planes of the support. The cobalt particle grew following an epitaxial relationship with the support, as both of them belong to the Fm3m cubic space group. In Fig. 7B, the cobalt planes are out of focus but the covering shell is now identified as poorly ordered carbon and C(002) planes are visible at 3.7 Å. Minor carbon deposition occurred on the surface of the CeO_2 support.

Small cobalt particles with cubic structure were also identified in the Co/Sm_2O_3 catalyst (see the high-resolution image in Fig. 8), where carbon deposition occurred almost exclusively on the Sm_2O_3 support (see inset in Fig. 8). Both Co/Sm_2O_3 and Co/CeO_2 catalysts showed minor

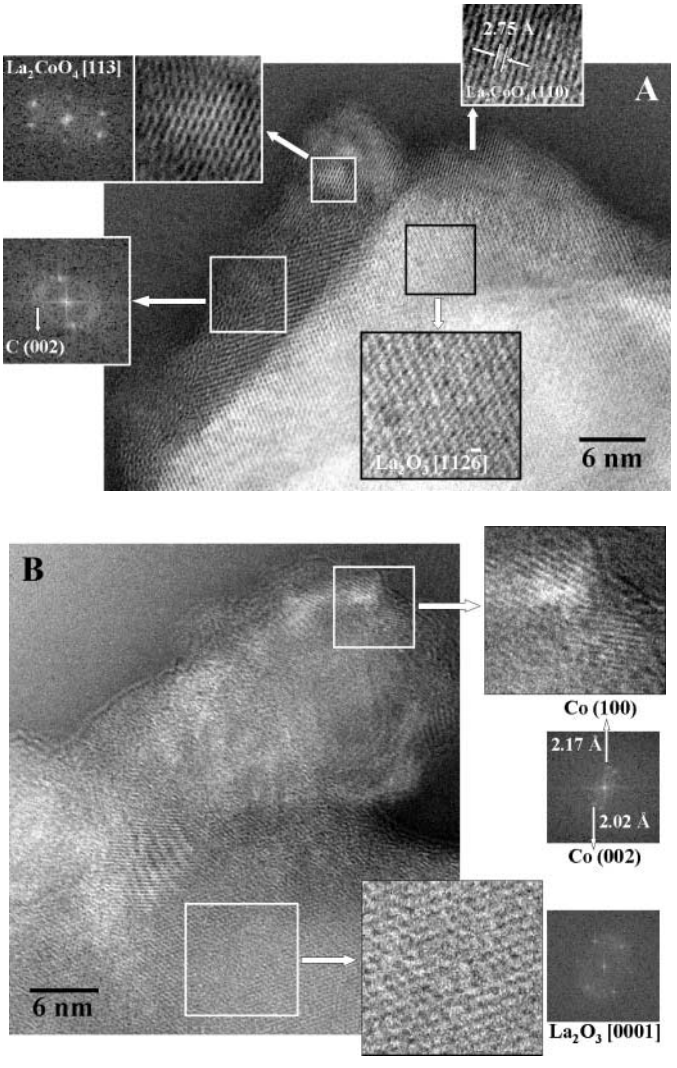

FIG. 5. High-resolution transmission electron microscopy images corresponding to the Co/La_2O_3 catalyst and derived Fourier transformed patterns. La_2CoO_4 spinel (A) and cobalt metal (B) particles are located in aggregates over La_2O_3 hexagonal crystals.

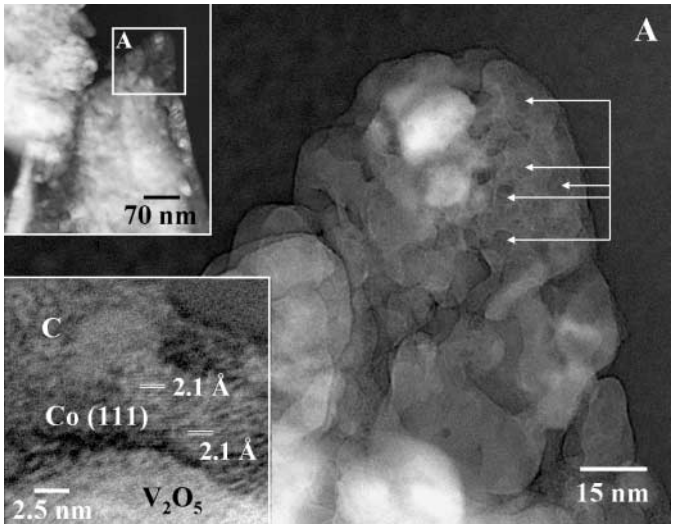

FIG. 6. Co/V_2O_5 catalyst. Extended carbon deposition is evident from transmission electron microscopy analysis (see, for example, inset A). Individual, 2- to 3-nm-size metal cobalt particles are present, which in turn are also covered by amorphous carbon.

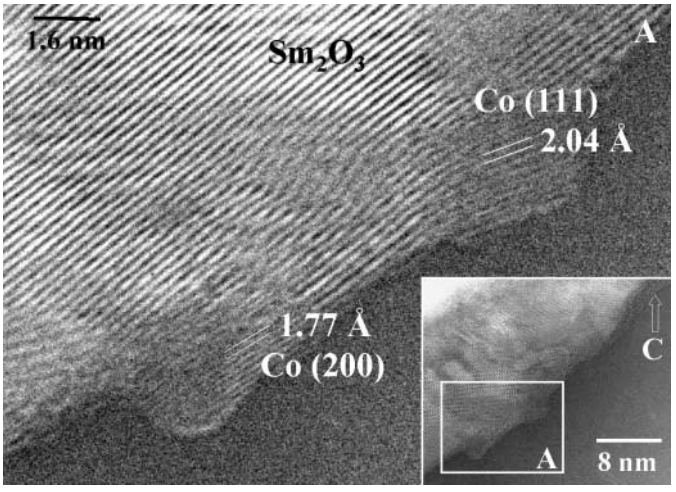

FIG. 8. Lattice-fringe images corresponding to the Co/Sm_2O_3 catalyst. Metal cobalt particles about 2 nm in size are supported on Sm_2O_3, as shown in inset A. Arrow marked as C in the low-magnification inset corresponds to carbon deposition on the support.

deactivation under reaction at 723 K. However, over Co/CeO_2 carbon deposited preferentially on metal cobalt particles whereas over Co/Sm_2O_3 carbon deposition took place largely on the support. This is in accordance with the higher deactivation and carbon deposition of Sm_2O_3 with respect to CeO_2 under similar reaction conditions (7).

Taking into account the fact that ZnO-supported catalysts showed the best catalytic performances, a more complete characterization of these samples after catalytic tests at different temperatures was done. On these samples, Co particles covered by highly disordered carbon phases and carbon deposition on the ZnO supports were identified. The morphology and extension of carbonaceous phases depended on the ZnO support and on the reaction temperature. It appears that carbon deposition on the high-surface ZnO-supported cobalt catalysts, Co/ZnO(2), was less pronounced than on the low-surface one, Co/ZnO(1). On the other hand a higher reaction temperature produced higher carbon deposition with more ordered structure.

Figure 9 displays a lattice-fringe image of the Co/ZnO(2) catalyst along with a low-magnification view. Metallic

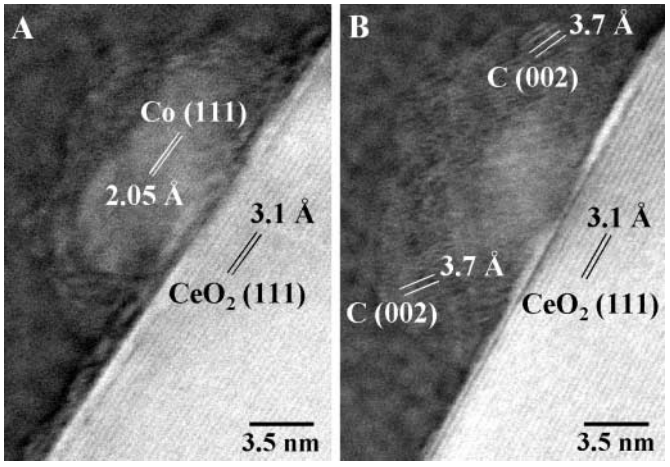

FIG. 7. High-resolution transmission electron microscopy images corresponding to the Co/CeO_2 catalyst in profile view. Figures A and B were obtained consecutively on the same area but under different focus conditions. A single metal cobalt particle exhibiting (111) planes has grown epitaxially on the CeO_2 support (A). On the other hand, poorly ordered carbon has developed onto the metal cobalt particle (B).

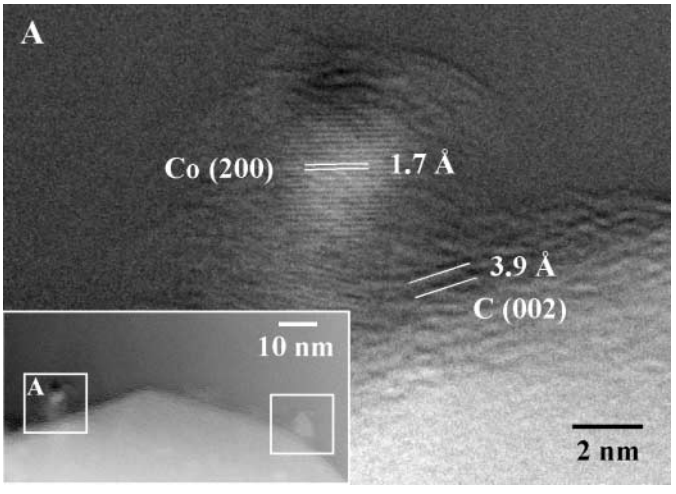

FIG. 9. Transmission electron microscopy images corresponding to Co supported on high-surface ZnO, Co/ZnO(2). Nanometer-size metal cobalt particles are well dispersed on ZnO. Highly disordered carbon is also present, as deduced from lattice-fringe imaging (inset A).

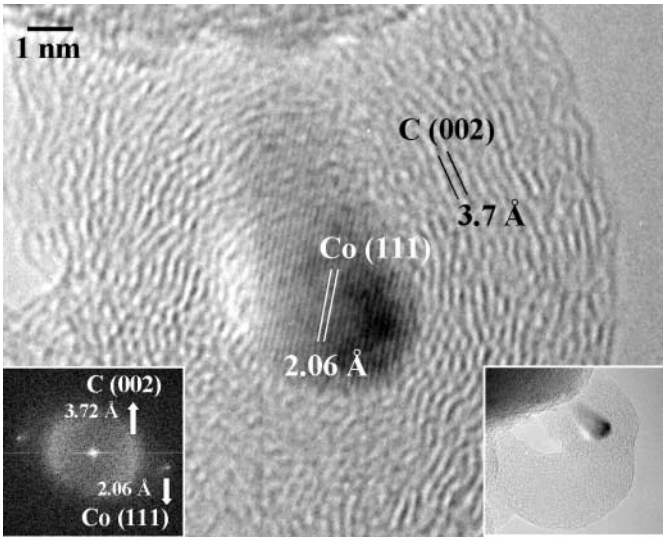

FIG. 10. Catalyst Co/ZnO(1) after reaction at 723 K. The occurrence of 3- to 4-nm-size metal cobalt particles through all the catalyst is clear from TEM. In all cases, metal cobalt particles appear covered by a poorly ordered carbonaceous phase. As is observed from Fourier transformed patterns, carbon deposition takes place to a larger extent on cobalt (111) planes (see inset).

cobalt particles with a cubic structure are located out of the support and are surrounded by amorphous carbon. Carbon deposition took place also on the ZnO support, but not in an organized way.

Co/ZnO(1) catalyst was characterized after reaction at 723 and 873 K. Figure 10 corresponds to the characterization of Co/ZnO(1) after reaction at 723 K. The high-resolution image shows a single metallic cobalt particle with a cubic structure surrounded by a poorly ordered carbonaceous phase with an onion-shell-type structure. The Fourier transformed image in the inset contains spots corresponding to Co(111) planes at 2.06 Å, as well as a diffuse ring at 3.72 Å corresponding to the (002) Miller indices of carbon. A C(002) spacing of 3.74 Å has been reported in the literature to represent a metastable carbon-rich phase related to the removal or formation of bonds or linkages during polymer carbonization (15). The diffuse ring is more dense in the direction of the Co(111) spots, indicating that the (002) crystallographic planes of carbon initially developed on the (111) planes of metallic cobalt. It appears that the growth of carbon was associated with the separation of metallic cobalt particles from the support.

When the reaction was carried out at 873 K over Co/ZnO(1), a strong change in the catalyst structure took place. Two different phenomena occurred. On one hand there was an abundant carbon deposition all over the catalyst with a more ordered structure and graphitic character with respect to the catalyst after reaction at 723 K. This is shown in Fig. 11, where a C(002) spacing of 3.46 Å is calculated directly from lattice-fringe imaging. In addition, there was the formation of carbon filaments containing cobalt particles much bigger than the metallic cobalt which remained in contact with the support: ca. 15–30 vs 3 nm (see inset in Fig. 11). The selected-area electron diffraction pattern included in the same figure shows single spots corresponding to a single metallic cobalt particle with cubic structure along with rings due to carbon. Now carbon rings are well-defined and constrained at 3.47 and 2.10 Å, which corresponds to the C(002) and C(100), C(101) planes, respectively. These values indicate a graphitic structure, which can range from 3.44 Å (interlayer spacing of randomly stacked graphitic layers) to 3.35 Å (fully ordered hexagonal graphite) (16). Similar spacing was obtained by X-ray diffraction at $2\theta \sim 25.7$ and 43.6 degrees, which corresponds to 3.46 and 2.08 Å, respectively.

Co/ZnO(1) catalyst was also characterized by TEM before catalytic reaction. We failed to identify any cobalt-based phase according to the preparation method of catalysts, which were tested after impregnation of $Co_2(CO)_8$ without previous calcination and/or reduction steps. This indicates that phases characterized after reaction were formed under reaction conditions and, according to the results, depended on the support characteristics. On some catalysts we detected cobalt particles after reaction. These catalysts showed a significant enhancement of the catalytic performance in the steam reforming of ethanol (see Table 1) when compared with the corresponding supports (7). However, from our results it was not possible to establish a relation between catalytic performance and cobalt particle size.

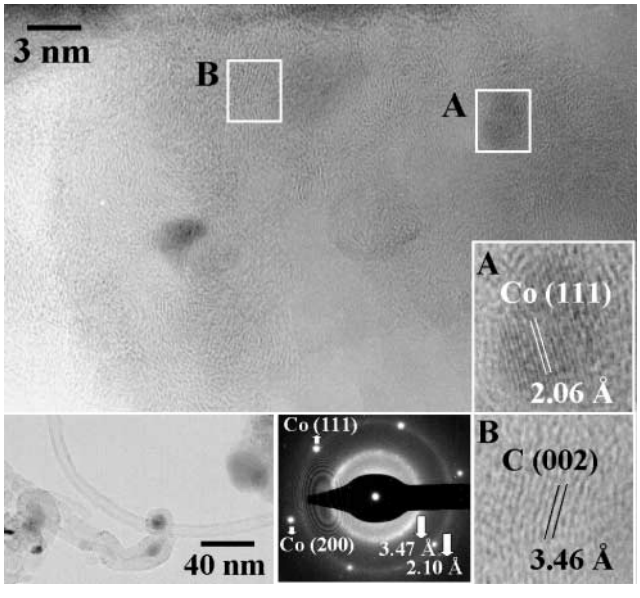

FIG. 11. Catalyst Co/ZnO(1) after reaction at 873 K. The size distribution of metal cobalt particles ranges from 3–4 nm up to 15–30 nm. Small metal cobalt particles are located on ZnO, whereas larger cobalt particles are located inside carbon filaments.

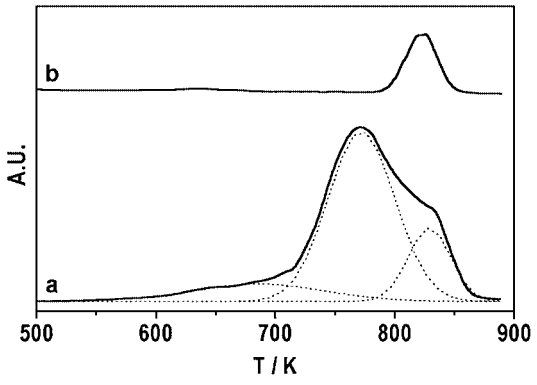

FIG. 12. Evolution of CH_4 obtained from temperature-programmed hydrogen reaction of the carbonaceous deposits formed on the Co/ZnO(1) catalyst. (a) After reaction at 723 K; (b) after reaction at 873 K.

More information about the nature of the carbonaceous deposits formed over Co/ZnO(1) was obtained by temperature-programmed hydrogen reaction (TPHR), X-ray photoelectron spectroscopy (XPS), and Raman spectroscopy.

TPHR was performed over the Co/ZnO(1) catalyst after reaction at 723 and 873 K. Both experiments were followed from 500 to 873 K. The evolution of methane, which was the only significant product evolved, is depicted in Fig. 12. The TPHR profile depended on the reaction temperature.

After reaction at 723 K (profile a), three peaks with maxima at 680 K (14% of total integrated area), 770 K (68% of total integrated area), and 830 K (18% of total integrated area) can be distinguished. The very broad signal centered at 680 K indicated the presence of relatively reactive carbon deposits on the catalyst, which may be identified as carbon in the β state (17). The other two signals, at 770 and 830 K, indicated the presence of amorphous carbon, which can be correlated with the poorly structured carbon deposition evidenced by TEM for this sample (Fig. 10).

The TPHR profile of catalyst after reaction at 873 K (profile b in Fig. 12) only showed a signal centered at 825 K, corresponding to the best structured amorphous carbon already shown by the sample after reaction at 723 K. Taking into account the temperature interval of TPHR experiments (500–823 K), these experiments did not show more ordered carbon, such as the filamentous structures observed by TEM in this sample (Fig. 11). Filamentous and platelet carbon exhibit peak temperatures of about 875 and 1120 K, respectively (17).

Figure 13 displays the X-ray photoelectron spectra recorded in the C 1s region over the Co/ZnO(1) catalyst after reaction at 723 and 873 K (spectra a and e, respectively). The C/Zn atomic ratio calculated for the catalyst reacted at 873 K is about 20 times greater than that corresponding to the catalyst after reaction at 723 K, in accordance with a major carbon deposition in the former, as evidenced by TEM.

Analysis of the profile corresponding to the catalyst after reaction at 723 K (Fig. 13, spectrum a) indicates the presence of four different types of surface carbon, with C 1s binding energies located at 284.4 (35%), 285.6 (38%), 286.8 (17%), and 289.8 (10%) eV. In contrast, the C 1s profile recorded for the catalyst after reaction at 873 K (Fig. 13, spectrum e) can be deconvoluted into two bands, centered at 284.4 eV (71%) and 285.5 eV (29%). C 1s BE values taken from the literature (18, 19) allow identification of the signal arising at 284.4 eV as due to graphene or graphitic carbon, whereas C 1s BE at ca. 285.6 eV is ascribed to aliphatic polymers. On the other hand, C 1s BE at 286.8 eV is typical of alcohol and keto surface groups, and that at 289.9 eV corresponds to carbonate species.

Figure 13 also shows XP spectra in the C 1s region of Co/ZnO(1) catalyst after reaction at 723 K and ulterior H_2 treatment at different temperatures, from 723 to 873 K (spectra b–d). An increase in thermal treatment with hydrogen produced the progressive diminution of bands at higher BE values. After a treatment under H_2 at 873 K, the C 1s spectrum profile (spectrum d) is similar to that obtained after the ethanol steam-reforming reaction at 873 K (spectrum e). The spectrum mainly shows a band located at 284.4 eV, associated with graphene or graphitic carbon. The band located at 285.5 eV significantly diminished after a H_2 treatment at 873 K, and it may be related to the carbon species showing a maximum of CH_4 evolution in the TPHR experiment at 770–830 K. As discussed above, the graphene/graphitic species responsible for the band at 284.4 eV will react with hydrogen at a higher temperature and is not visible in the TPHR experiment.

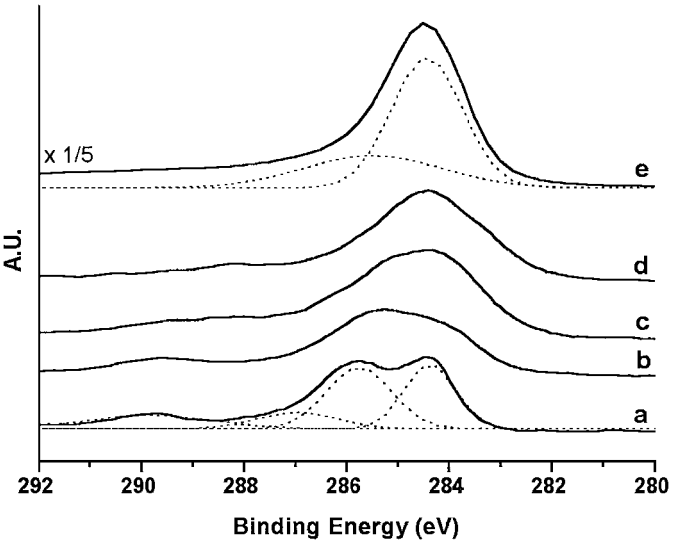

FIG. 13. X-ray photoelectron spectra in the C 1s region corresponding to the Co/ZnO(1) catalyst. (a) After reaction at 723 K; (b), after (a), H_2 treatment at 723 K; (c) after (b), H_2 treatment at 800 K; (d) after (c), H_2 treatment at 873 K; (e) after reaction at 873 K.

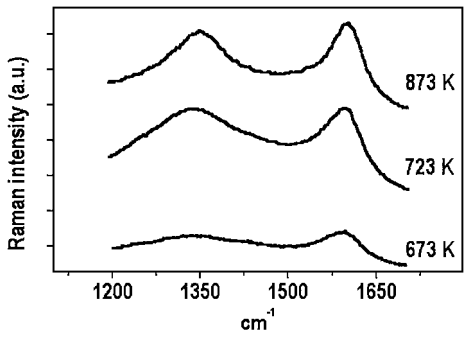

FIG. 14. Raman spectra in the carbon region obtained for catalyst Co/ZnO(1) after reaction at different temperatures.

The Raman spectra in the range 1200–1700 cm^{-1} of the sample Co/ZnO(1) after reaction at 723 and 873 K are presented in Fig. 14. Two distinctive bands are visible in each spectrum, at 1339–1345 (D line) and 1592–1597 cm^{-1} (G line). These two bands are very sensitive to the extent of two-dimensional graphitic ordering and have been used extensively to study disorder in carbon deposits (20). The bands in our spectra are relatively broad, indicating a large degree of interstitial disorder, that is, along the *c*-axis between the in-plane direction. The spectroscopic parameters obtained after curve fitting for each spectrum are compiled in Table 3.

A quantitative characterization of the degree of disorder in carbonaceous materials can be made on the basis of the integrated intensity of the D and G lines, as well as their relative width and frequency. The microcrystalline planar size L_a shows a linear relationship with the ratio of the integrated intensity of G vs D line: $L_a = 44(I_G/I_D)$ (21). When the ethanol-reforming reaction is carried out over the Co/ZnO(1) catalyst, the resulting L_a value is about 0.9 nm at 723 and 1.4 nm at 873 K. Both values indicate a large degree of disorder compared to values reported in the literature for other cobalt-based catalysts in different reactions (22), suggesting that a very poorly graphitized structure was developed on the ZnO-supported catalyst in our experiment. On the other hand, when the reaction temperature was increased from 723 to 873 K, a certain ordering of the carbonaceous deposit took place with respect to the structure, resulting from reaction at 723 K, as deduced from an increase of the L_a value. This is also reflected by an increase in the frequency of the D and G lines, as well as by a decrease in their bandwidth; see Table 3).

Raman results are in close agreement with TEM data discussed above and illustrated in Figs. 10 and 11 and with XP spectra and TPHR experiments. The higher the ethanol steam-reforming reaction temperature, the larger the amount of carbon deposits with increasing ordering.

Finally, in Fig. 14 and Table 3 also appear the Raman results for the Co/ZnO(1) catalyst, characterized after a separate catalytic test carried out at 673 K for 50 h. The characteristics of the bands and the L_a value obtained confirm that a lower amount of carbonaceous deposit with a lower order is obtained after a catalytic test at a lower temperature.

TABLE 3

Raman Spectroscopic Parameters Obtained after Curve Fitting the Experimental Spectra by Using Two Lorentzian Bands (Bands G and D) of Catalyst Co/ZnO(1) after Reaction at Different Temperatures

Reaction T (K)	Peak position[a] (cm^{-1})	FWHM (cm^{-1})	L_a (nm)[b]
673	1337 (88)	190	0.6
	1592 (12)	60	
723	1339 (83)	177	0.9
	1592 (17)	50	
873	1345 (76)	130	1.4
	1597 (24)	41	

[a] Values in parentheses represent the percentage area of each peak after deconvolution.

[b] Microcrystalline planar size calculated from $L_a/Å = 44(I_G/I_D)$ (21).

CONCLUSIONS

A positive effect of cobalt addition to several oxides in the catalytic production of hydrogen from ethanol aqueous solutions has been shown. Catalysts containing cobalt particles showed a significant enhancement of the catalytic performance in the steam reforming of ethanol compared with the corresponding supports. The extent and degree of ordering of carbon deposits that occur during reaction depend on the material and the reaction temperature. The higher the temperature, the higher the extension and order of the carbonaceous phase.

ACKNOWLEDGMENTS

We thank CICYT (MAT1999-0477) and Generalitat de Catalunya (1999 SGR-00044) for financial support. J. Ll. is grateful to MCYT for a Ramón y Cajal Research Program.

REFERENCES

1. Peña, M. A., Gomez, J. P., and Fierro, J. L. G., *Appl. Catal. A* **144**, 7 (1996).
2. Breen, J. P., and Ross, J. R. H., *Catal. Today* **51**, 521 (1999).
3. Velu, S., Suzuki, K., and Osaki, T., *Chem. Commun.* 2341 (1999).
4. Takezawa, N., and Iwasa, N., *Catal. Today* **36**, 45 (1997).
5. Haga, F., Nakajima, T., Miya, H., and Mishima, S., *Catal. Lett.* **48**, 223 (1997).
6. Amphlett, J. C., Leclerc, S., Mann, R. F., Peppley, B. A., and Roberge, P. R., *in* "Proc. Intersoc. Energy Conver. Eng. Conf., 33rd, Colorado Springs," Paper no. 98-269. Society of Automotive Engineers, Warrendale, PA, 1998.
7. Llorca, J., Ramírez de la Piscina, P., Sales, J., and Homs, N., *Chem. Commun.* 641 (2001).
8. Llorca, J., Barbier, A., Martin, G. A., Sales, J., Ramírez de la Piscina, P., and Homs, N., *Catal. Lett.* **42**, 87 (1996).

9. Topsoe, N., and Topsoe, H., *J. Catal.* **75**, 354 (1982).
10. Kung, H. H., *Stud. Surf. Sci. Catal.* **45**, 146 (1989).
11. Nakajima, T., Yamaguchi, T., and Tanabe, K., *J. Chem. Soc. Chem. Commun.* 394 (1987).
12. Murthy, R. S., Patnaik, P., Sidheswaran, P., and Jayamani, M., *J. Catal.* **109**, 298 (1988).
13. Arnoldy, P., and Moulijn, J. A., *J. Catal.* **93**, 38 (1985).
14. Cimino, A., and Stone, F. S., *in* "Handbook of Heterogeneous Catalysis" (G. Ertl, H. Knözinger, and J. Weitkamp, Eds.), Vol. 2, p. 845. Wiley–VCH, Weinheim, 1997.
15. Rietmeijer, F. J. M., *Carbon* **29**, 669 (1991).
16. Jenkins, G. M., and Kawamura, K., "Polymeric Carbons—Carbon Fibre, Glass and Charcoal." Cambridge Univ. Press, Cambridge, UK, 1976.
17. McCarty, J. G., Hou, P. Y., Sheridan, D., and Wise, H., *in* "Coke Formation on Metal Surfaces" (L. F. Albright and R. T. K. Baker, Eds.), ACS Symposium Series 202, p. 253. Am. Chem. Soc., Washington, DC, 1982.
18. Rodriguez, N. M., Anderson, P. E., Wootsch, A., Wild, U., Schlögl, R., and Páal, Z., *J. Catal.* **197**, 365 (2001).
19. Schlögl, R., in "Handbook of Heterogeneous Catalysis" (G. Ertl, H. Knözinger, and J. Weitkamp, Eds.), Vol. 1, p. 138. Wiley–VCH, Weinheim, 1997.
20. Lespade, P., Marchand, A., Couzi, M., and Cruege, F., *Carbon* **22**, 375 (1984).
21. Tuinstra, F., and Koenig, J. L., *J. Chem. Phys.* **53**, 1126 (1970).
22. Pinheiro, P., Schouler, M. C., Gadelle, P., Mermoux, M., and Dooryhée, E., *Carbon* **38**, 1469 (2000).